Seismic wide-angle processing to avoid stretch

Fred J. Hilterman* and Connie J. VanSchuyver*

**** formerly Geophysical Development Corporation, currently University of Houston***

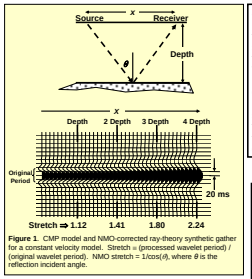

Figure 1. CMP model and NMO-corrected ray-theory synthetic gather for a constant velocity model. Stretch = (processed wavelet period) / (original wavelet period). NMO stretch = $1/\cos(\theta)$, where θ is the reflection incident angle.

Summary

A processing and interpretation approach has been developed that avoids NMO stretch for a specified target horizon. We call this approach Seismic Wide-Angle Processing (SWAP)TM. Both conventional pre-stack attributes and high-resolution attributes for seismic data at offsets greater than twice the depth of the target horizon are generated. There are two essential steps that are different from conventional processing. The first is a pre-stack migration in the common-offset domain that maintains the same common-offset after migration. That is, NMO corrections are removed from migration. The second is a NMO correction that is centered on the target horizon. Static shifts based on a ray-trace model to the target horizon provide the NMO corrections for all offsets. Only the target horizon is truly flat in the CDP gathers after applying the static shifts. The resulting offset volumes contain target-horizon events that essentially have the same frequency content as the near-offset volume. Interpretation is limited to approximately 200 ms around the target horizon. Initial tests indicate that both structural and amplitude interpretations are improved on offsets greater than twice the depth of the target horizon.

Introduction

With the introduction of anisotropic NMO, CDP traces are routinely processed that have offsets approaching twice the depth (Hilterman et al., 2000). With the inclusion of these large offsets, amplitude interpretation of pore-fluid content is greatly enhanced. However, the frequency content of the seismic wavelet is reduced on the far offsets and AVO inversions become problematic. This loss in frequency content is primarily associated with NMO corrections. Various approaches for removing NMO stretch have been outlined by Hicks, 2001a and 2001b. However, there is an offset limit where these approaches become impractical. In addition, the NMO stretch associated with migration was not addressed.

There are numerous motivations for having the same seismic wavelet on the near traces as on the far-offset traces. A few are:

- Robust AVO inversions,
- Single wavelet inversion for EI,
- High-resolution fracture detection,
- Detection of channel cuts that exhibit anomalous amplitudes on offsets greater than twice the depth,
- Analysis of converted-wave energy on PP reflections past 35° incident angles, and
- Recognition of head-wave events and its properties.

The goal is to provide a migration scheme that preserves the recorded seismic wavelet independent of the source-receiver offset. Then, provide an interpretation and processing approach that preserves the frequency content on angle stacks significantly past offset = depth.

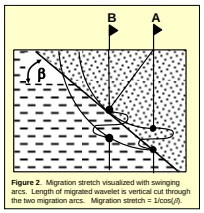

Figure 2. Migration stretch visualized with swinging arcs. Length of migrated wavelet is vertical cut through the two migration arcs. Migration stretch = $1/\cos(\beta)$.

Method

While migration is performed before NMO corrections in wide-angle processing, NMO will be discussed first. In Figure 3, synthetic CDP gathers are displayed after NMO corrections. Figure 3A displays a P-wave primary-only ray-trace synthetic. After filtering, NMO corrections were applied based on ray-trace times. The high-velocity layer at 1820 ms (arrow annotation) is muted as the critical angle is approached, which is at approximately offset = 1.5 depth. NMO stretch is evident near the mute zone. Figure 3b contains a synthetic for the same well that was generated with the total elastic algorithm (SLID, Sherwood et al, 1983). Besides the obvious NMO stretch at offsets greater than twice the depth, a reversal of NMO traveltimes creates a non-usable zone that is normally muted. Associated with this non-useable zone in Figure 3b is a high-amplitude event from the high-velocity layer that appears to be under-corrected. The desire is to preserve this event without NMO stretch. In Figure 3c, the same elastic synthetic was flattened on the 1820 ms event using static shifts derived by ray-tracing. Only the target event at 1820 ms is truly flat on this CDP gather. The wavelet associated with the reflection at 1820 ms in Figure 3c has the same frequency content for offsets from zero to three times the depth. Reflections past the critical angle are maintained. Because static corrections for the 1820 ms event were applied, the events above 1820 ms appear under-corrected and those below, over-corrected.

If NMO is applied during migration, the non-usable zone beyond offsets that are twice the depth in Figure 3b will be present. Thus, a migration process that can be applied to all common-offset volumes without NMO corrections is desired. In Figure 4, conventional Kirchhoff migration is cartooned. Energy from the unmigrated input trace A is mapped into the migrated output trace I. Trace A has an offset X. Based on the t_0 time of output trace I, energy from trace A at t_{MIG} is moved to t_0, where $t_{MIG} = t_I + t^2$. This operation performs both the NMO correction and migration. In order to remove the NMO correction, the energy on the migrated trace at t_0, which comes from trace A, is moved to t_{UNMO}, where $t_{UNMO} = t_I + t_N$. The velocity control is $V_I(t_0)$ for both the input and output traces. The energy on trace I at t_{UNMO} is migrated but still has NMO based on the original offset X and the velocity $V_I(t_0)$.

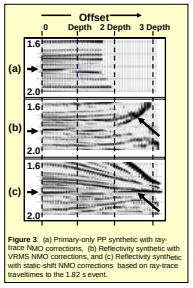

Figure 3. (a) Primary-only PP synthetic with ray-trace NMO corrections, (b) Reflectivity synthetic with VRMS NMO corrections, and (c) Reflectivity synthetic with static-shift NMO corrections based on ray-trace traveltimes to the 1.82 s event.

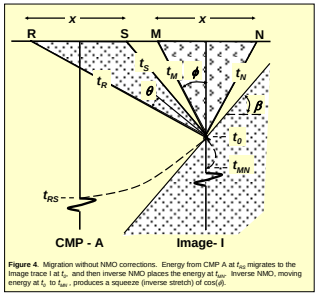

Figure 4. Migration without NMO corrections. Energy from CMP A at t_{RS} migrates to the Image trace I at t_0, and then inverse NMO places the energy at t_{MN}. Inverse NMO, moving energy at t_0 to t_{MN}, produces a squeeze (inverse stretch) of $\cos(\phi)$.

In Figure 4, the removal of the NMO correction can be inferred to be a separate step after conventional Kirchhoff migration. The actual implementation cannot be performed as such. An aspect of this migration technique is that the process of filling the output trace is not based on a sample indexing of the output trace. Instead, increment t0, find the amplitude on trace A at t_{MIG} and place it in the output trace at t_{UNMO}. As t_0 increases, the times $t_{UNMO}(t_0)$ can decrease, thus giving rise to crossing events in the final CDP gather. The double-valued times in the t_{UNMO} array allow crossing events in the original input gather to remain crossing after migration. In other words, if there were no dip, the migrated gather would be a duplicate of the input unmigrated gather with no NMO corrections.

This migration requires counting the number of traces added to each time sample in the migrated trace I.

After migration and flattening of the target horizon in the CDP gather, the gather can be transformed from the offset domain to the incident-angle domain. With the depth model of the target horizon known, more accurate estimates of incident angles on the target horizon can be assigned to each offset.

An abbreviated summary of the wide-angle processing is:

1. Conventional velocity and anisotropy analyses,
2. Non-NMO migration with anisotropy,
3. Import of interpreter's target horizon arrival times,
4. Ray-trace static corrections for flattening target horizon in the CDP gathers,
5. Trim static to "absolutely" flatten target horizon in CDP gather,
6. Incident-angle gathers based on ray-trace model of target horizon,
7. AVO inversion, angle-limited stacks, etc., and
8. Final volume(s) displayed at target horizon time.

The trim-static corrections derived in Step 5 can be used to upgrade both the velocity and anisotropy models.

Conventional stacks and AVO products can also be derived from the non-NMO migration by applying regular NMO corrections.

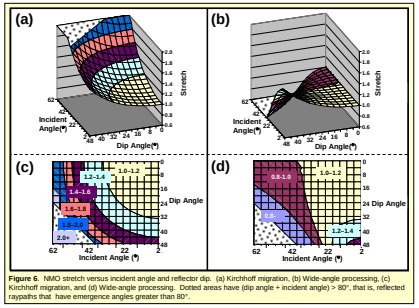

Figure 6. NMO stretch versus incident angle and reflector dip. (a) Kirchhoff migration, (b) Wide-angle processing, (c) Kirchhoff migration, and (d) Wide-angle processing. Dotted areas have (dip angle + incident angle) > 80°, that is, reflected raypaths that have emergence angles greater than 80°.

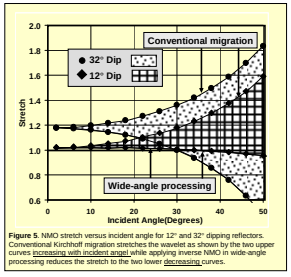

Figure 5. NMO stretch versus incident angle for 12° and 32° dipping reflectors. Conventional Kirchhoff migration stretches the wavelet as shown by the two upper curves increasing with incident angel while applying inverse NMO in wide-angle processing reduces the stretch to the two lower decreasing curves.

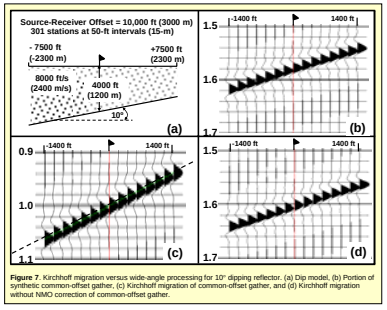

Figure 7. Kirchhoff migration versus wide-angle processing for 10° dipping reflector. (a) Dip model, (b) Portion of synthetic common-offset gather, (c) Kirchhoff migration of common-offset gather, and (d) Kirchhoff migration without NMO correction of common-offset gather.

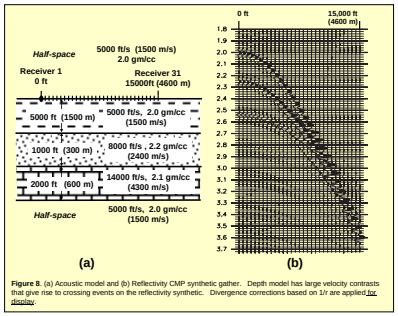

Figure 8. (a) Acoustic model and (b) Reflectivity CMP synthetic gather. Depth model has large velocity contrasts that give rise to crossing events on the reflectivity synthetic. Divergence corrections based on 1/r are applied for display.

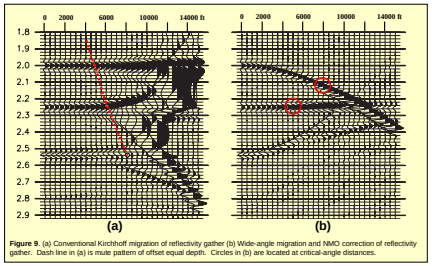

Figure 9. (a) Conventional Kirchhoff migration of reflectivity gather (b) Wide-angle migration and NMO correction of reflectivity gather. Dash line in (a) is mute pattern of offset equal depth. Circles in (b) are located at critical-angle distances.

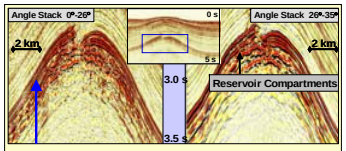

Figure 10. Prestack time migrations with conventional near-angle stack (0°-26°) and far-angle stack (26°-35°). Structure is a faulted anticline with some indication of fault blocks near the apex. Potential reservoirs are within the high-amplitude band. The small insert illustrates the total relief of the anticline.

Discussion

Because NMO in performed after a target horizon is specified, interpretation of wide-angle processed data requires an interface between the processing system and the interpretation workstation. All migrated offset volumes need to be accessed after specifying a target horizon.

If an angle range is stacked then subsequent interpretation is limited to the specified target horizon and events that are approximately 200 ms around the target horizon. This is due to the under- and over-corrected events around the target horizon as illustrated in Figure 3c.

Conclusions

In this study, a processing procedure is presented that preserves the frequency content of a reflection event from near angles to angles associated with offsets three times the depth. The suggested migration algorithm is implicit and does not depend on the target horizons. Thus, migration only has to be done once and them numerous target horizons can be examined.

Benefits that have been shown from horizon processing are:

- Improved S/N ratio on stacks,
- Improved amplitude control for AVO analyses,
- Improved structural information,
- Improved inversion for elastic impedance,
- Update of velocity and anisotropy models, and
- Preservation of frequency content.

In addition, wide-angle processing provides the interpreter with a new data set that previously has not been available for detecting subtle variations at boundary interfaces associated with incident-angle obliquity.

Acknowledgements

The authors are grateful to Statoil for permission to show the field data, and in particular, we appreciate the valuable input from J.R. Granli and R.J. Fredsted (Statoil). Peg Guthrie and Kevin Chesser provided petrophysical and modeling support, Luh Liang, Chung Lui, Karl Schleicher and Juhn DuBose provided theoretical and programming support.

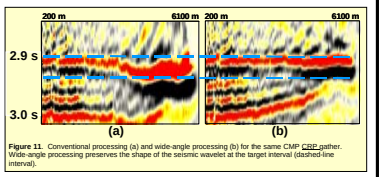

Figure 11. Conventional processing (a) and wide-angle processing (b) for the same CMP CRP gather. Wide-angle processing preserves the shape of the seismic wavelet at the target interval (dashed-line interval).

Example

Figure 10 illustrates a 0°-26° angle stack that traverses a large faulted anticline. Potential hydrocarbon zones are located within the high-velocity anhydrite beds that give rise to the high-amplitude events on the section.

Besides the obvious fault at the crest of the structure, other fault-block compartments are believed to be near the crest. To illustrate the frequency resolution, the structure in Figure 10 was flattened on the upper high-amplitude event. A far angle stack (30°-50°) is then displayed in Figure 12b. This section has undergone conventional processing.

The low frequency content on the 30°-50° angle stack (Figure 12b) makes both structural and amplitude interpretation impossible. The jumps in event continuity on the flat event for the 30°-50° angle stack occur at velocity control points. This is a variation in the wavelet spectrum and indicates that a single wavelet can't represent the far-offset angle stack for subsequent EI inversions.

In figure 12c, the same angle stack as shown in Figure 12b is displayed after wide-angle processing. The frequency content of the seismic wavelet at the target interval is essentially the same on the near-incident angle stack (Figure 12a) as on the far incident-angle stack (Figure 12c). For the far-angle stack, both structural and amplitude interpretations of the target horizon are now possible. In fact, fault blocks are clearly defined on the 30°-50° angle stack (Figure 12c). The same fault blocks are more difficult to observe on the near-angle stack (Figure 12a).

In order to illustrate the robustness of the seismic wavelet with offset, the two angle stacks in Figure 12a and c were inverted using the same seismic wavelet. The inversions are shown in Figure 14. The character of the inverted traces on the near and far angle stacks is essentially the same.

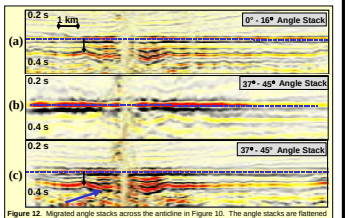

Figure 12. Migrated angle stacks across the anticline in Figure 10. The angle stacks are flattened on the horizon of interest to illustrate wavelet-frequency preservation of the target horizon. The angle stack (37°-45°) was processed conventionally (b) and wide angle (c). Fault-block delineation is better in far-angle stack (c) than on the near-angle stack (a).

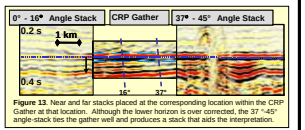

Figure 13. Near and far stacks placed at the corresponding location within the CRP Gather at that location. Although the lower horizon is over corrected, the 37°-45° angle-stack ties the gather well and produces a stack that aids the interpretation.

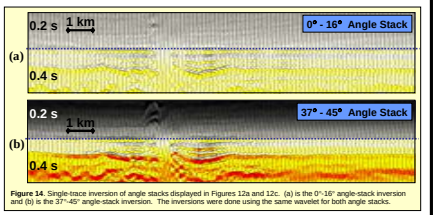

Figure 14. Single-trace inversion of angle stacks displayed in Figures 12a and 12c. (a) is the 0°-16° angle-stack inversion and (b) is the 37°-45° angle-stack inversion. The inversions were done using the same wavelet for both angle stacks.

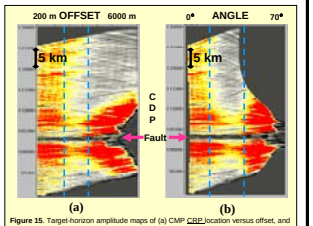

Figure 15. Target-horizon amplitude maps of (a) CMP CRP location versus offset, and (b) CMP CRP location versus incident-angle. Target horizon is indicated by dotted line in Figure 12.